Systematic study on the removal of per- and polyfluoroalkyl substances from contaminated groundwater using metal-organic frameworks

Rui Li[1,2*], Shefa Alomari[3], Timur Islamoglu[4], Omar K. Farha[4,5], Sujan Fernando[2], Selma Mededovic Thagard,[1] Thomas M. Holsen,[6] and Mario Wriedt[3*]

[1]Department of Chemical and Biomolecular Engineering, Clarkson University, Potsdam, New York 13699, USA

[2]Center for Air and Aquatic Resources Engineering & Science, Clarkson University, Potsdam, New York, 13699, USA

[3]Department of Chemistry & Biomolecular Science, Clarkson University, Potsdam, New York 13699, USA

[4]International Institute of Nanotechnology, Department of Chemistry, Northwestern University, Evanston, Illinois 60208, USA

[5]Department of Chemical and Biological Engineering, Northwestern University, Evanston, Illinois 60208, USA

[6]Department of Civil and Environmental Engineering, Clarkson University, Potsdam, New York 13699, USA

Corresponding authors

RL, Email: rli2@clarkson.edu; Tel: 315-268-3851

MW, Email: mwriedt@clarkson.edu; Tel: 315-268-2355

ABSTRACT

Harmful per- and polyfluoroalkyl substances (PFAS) are ubiquitously detected in aquatic environments but their remediation remains challenging. Metal-organic frameworks (MOFs) have been recently identified as advanced material class for efficient removal of PFAS, but little is known about the fundamentals of the PFAS@MOF adsorption process. To address this knowledge gap, we evaluated the performance of three different MOFs for the removal of eight PFAS classes from aqueous film-forming foam-impacted groundwater samples obtained from eleven U.S. Air Force installations. Due to their different pore size/shape and identity of metal node, MOFs NU-1000, UiO-66, and ZIF-8 were selected to investigate the role of MOF structures, PFAS properties and water matrix on the PFAS@MOF adsorption process. We observed that PFAS@MOF adsorption is (i) dominated by electrostatic and acid-base interactions for anionic and non-ionic PFAS, respectively, (ii) preferred for long- over short-chain PFAS, (iii) strongly dependent on the nature of PFAS head group functionality, and (iv) compromised in the presence of ionic and neutral co-contaminants by competing for ion-exchange sites and PFAS binding. With this study we elucidate the PFAS@MOF adsorption mechanism from complex water sources to guide the design of more efficient MOFs for treatment of PFAS contaminated water bodies.

Keywords: adsorption mechanism; groundwater matrix; metal-organic frameworks; per- and polyfluoroalkyl substances.

SYNOPSIS

This work investigates metal-organic frameworks for the adsorption of PFAS from complex water sources to guide the design of more efficient adsorbents for contaminated water remediation.

INTRODUCTION

Per- and polyfluoroalkyl substances (PFAS) have a wide variety of industrial and commercial applications including their use in semiconductor manufacturing, aqueous film-forming foam (AFFF) for firefighting activities, and surface coating for non-stick cookware, among other applications.[1–3] Due to their highly persistent nature, PFAS are ubiquitously detected in groundwater, surface and tap water; they also accumulate at significant levels in wildlife and humans.[4] An increasing concern about the effects of PFAS on environmental and human health motivated researchers from federal agencies, industrial and academic groups around the globe to investigate the extent of PFAS contamination. The development and purge water from the installation and sampling of monitoring wells at these AFFF-impacted sites generates significant amounts of liquid investigation-derived waste (IDW) which contains a complex mixture of diverse classes of PFAS.[5] Thus, there is an urgent need for the effective and efficient remediation of PFAS-contaminated groundwater at AFFF-impacted sites.

Significant attention has been focused on treatment technologies for PFAS removal from groundwater with adsorption-based processes being among the most effective approaches.[6,7] To date, granular activated carbons (GAC) and ion exchange (IX) resins are the most commonly used adsorbents for PFAS removal from groundwater.[8,9] Despite its high selectivity towards long-chain PFAS, GAC shows low adsorption capacity, slow mass transport, and poor performance for short-chain PFAS.[6,10] IX resins are an alternative sorbent for PFAS removal. However, the time to reach adsorption equilibrium is usually long (50 - 168 h) and they are not effective at removing non-ionic PFAS such as perfluoroalkane sulfonamide (FOSA).[11,12] The development of novel adsorbents featuring high selectivities for different PFAS classes along with high adsorption capacities and fast adsorption kinetics is therefore of great importance.

Metal-organic frameworks (MOFs) are porous, crystalline materials composed of inorganic nodes and organic linkers that assemble into multidimensional lattices through coordination bonds.[13–15] The unique characteristics of MOFs such as ultra-high surface areas and pore volumes combined with their structural tunability render them as promising candidates for the adsorption and/or separation of small

molecules.[16–22] Rapid adsorption kinetics are commonly found within such applications making MOFs particularly promising candidate materials for water remediation. For example, MOFs have been proven to be effective in removing a wide range of pollutants from water including heavy metals, dyes, and pharmaceuticals.[13,23,24] However, the application of MOFs for PFAS removal is underexplored.[25] The few existing PFAS@MOF studies focus on the adsorption of perfluorooctanoic acid (PFOA) and perfluorooctanesulfonic acid (PFOS), two well-known long-chain perfluoroalkyl acids (PFAA), but the performance of MOFs on short-chain PFAS is unclear.[26–34] Furthermore, there are nearly 5000 different types of PFAS and the role of their charge state, chain length and head group functionality on the adsorption behavior using MOFs is largely unknown. Finally, the few existing PFAS@MOF studies are performed using laboratory-prepared simulants, thus, the complexity of the water matrix found in samples from AFFF-impacted sites is not reflected, which is known to significantly affect the performance of adsorbents.

Herein, we report the role of water matrix, chain length, functional group and charge state of PFAS on the adsorption behavior of three different MOFs. MOFs NU-1000,[35] UiO-66,[36] and ZIF-8[37] were selected based on their variety of structural features (i.e., metal node composition, nature of organic linkers, pore sizes and pore topologies). We investigated these MOFs for their removal efficiency of eight classes of PFAS from AFFF-contaminated groundwater samples. Their selectivity towards anionic and non-ionic PFAS was compared with the adsorption characteristics of commercial GAC while the role of PFAS chain length, functional group, and water matrix on PFAS adsorption was investigated for selected MOFs. To the best of our knowledge, this is the first study that uses MOFs to explore the removal of a wide range of PFAS from contaminated groundwater samples.

MATERIALS AND METHODS

Chemicals. Mixed, individual, and labeled internal standards were purchased from Wellington Laboratories (Guelph, ON) and 3M (St. Paul, MN) as listed in **Table S1**. Methanol, water, and acetonitrile

(LC-MS grade) were purchased from Thermo Fisher Scientific (Waltham, MA). Ammonium acetate (LC-MS grade) was purchased from Sigma Aldrich (St. Louis, MO).

Absorbents. MOFs NU-1000, UiO-66, and ZIF-8 were synthesized according to published methods;[38–42] and commercial GAC (FILTRASORB 300) was obtained from Calgon Carbon (Moon Township, PA).

Groundwater samples. Eleven PFAS contaminated groundwater samples were collected in 2019 at different locations from monitoring wells in fire training areas, burn pits, and various other water sources as a part of completed field investigations at U.S. Air Force installations.[5] The samples were collected in 18.9 L high density polyethylene (HDPE) containers, secured in coolers, and shipped to Clarkson University packed on ice. Samples were stored at 4 °C upon receipt and labeled as IDW 1 through IDW 11 to maintain the confidentiality of sample locations. Their detailed characteristics are listed in **Table S2.**

Batch experiments. Adsorption studies were performed by exposing 10 mg of adsorbent to 50 mL of IDW in a 50 mL polypropylene tube which was mixed on a tumbler at 150 rpm at room temperature. To evaluate the effect of the MOF structures on PFAS adsorption, IDW 6 was treated for 30 min by NU-1000 and sampled at 1, 2 and 30 min. IDW 6 was treated for 48 h by UiO-66 and ZIF-8 and sampled at 1 min, 10 min, 30 min, 24 h and 48 h. IDW 6 was treated for 28 h by GAC and sampled at 1, 2, 24 and 48 h. To evaluate the role of water matrix on PFAS adsorption, IDWs 1 to 11 were treated by NU-1000 for 30 min. A control experiment was performed without adsorbents to evaluate the loss from adsorption on tubes and filters for IDW 6 for 48 h. All samples were filtered with a 0.25 μm nylon membrane and diluted using methanol before analysis. Before treatment, soil particles in the IDW samples were allowed to settle in their original containers. The supernatant was then transferred to a 1-L HDPE container, sonicated and vortexed before batch adsorption experiments. No other pretreatment was performed. All experiments were performed in duplicate and average values were reported.

Analytical procedure. The concentrations of 26 PFAS were measured in the negative ionization mode using a UPLC-MS-MS (Thermo Scientific, Vanquish-TSQ ALTIS) equipped with a Phenomenex Luna

Omega column (2.1 mm × 100 mm, 1.6 μm). Samples were diluted with methanol in 1:1 v/v ratio (9:1 for IDW 11 due to the high PFAS concentrations), then sonicated and centrifuged prior to injection (5 μL). A detailed description of the analytical method is provided in **Text S1** and **Tables S3-S4.** For QA/QC, all filtered samples were spiked with 2 ng of labeled internal standards. An eight-point calibration in the range of 9 to 20000 ng/L was used for quantification using an internal standard calibration. Quantification was performed only when the standards yielded a regression fit of $r^2 > 0.99$ and deviation < 30%, and surrogate recovery was between 70 and 120%. Detection limits were in the range of 3 - 17 ng/L. Two PFAS (PBSaAm and PFHxSaAm) were analyzed in the positive mode using the same LC parameters and quantified by external calibration. Total organic carbon (TOC) concentration was measured using a TOC analyzer (Shimadzu, TOC-VCPH). Solution electrical conductivity and pH were measured using probes (YSI, MultiLab IDS 4010-2). Turbidity was measured using a turbidity meter (Hach, 2100N). Total alkalinity and hardness were measured following standard methods (APHA, 2017).

Statistical analysis. Statistical analyses were performed with Python software (version 3.8) with statistical difference set at $p < 0.05$. A Spearman correlation was used to compare the role of water matrix on PFAS removal.

RESULTS AND DISCUSSION

PFAS concentration in IDW water samples. A total of 28 PFAS compounds were detected in water samples IDW 1-11 with ∑PFAS concentrations ranging from 2.1 μg/L for IDW 8 to 350 μg/L for IDW 11. The mean ∑PFAS concentration is 190 ± 250 μg/L. **Figure 1** with **Tables S2** and **S5** show the detailed composition and characteristics of all water samples. The detected PFAS belong to eight PFAS classes including (i) perfluorinated carboxylic acid (PFCA), (ii) perfluorosulfonic acid (PFSA), (iii) fluorotelomer sulfonic acid (FTS), (iv) fluorotelomer carboxylic acid (FTCA), (v) perfluoroalkane sulfonamide acetic acid (FASAA), (vi) perfluoroalkane sulfonamide (FASA), (vii) N-methyl perfluoroalkane sulfonamide

(MeFASA) and (viii) N-[3-(dimethylamino)propyl]-perfluoroalkane sulfonamide (Am-Pr-FASA). Their mean concentrations are 38 ± 53, 78 ± 120, 26 ± 54, 0.26 ± 0.45, 0.09 ± 0.16, 51 ± 53, 0.01 ± 0.02 and 0.08 ± 0.14 μg/L, respectively. Of the 28 PFAS analyzed, PFBA, PFPeA, PFHxA, PFHpA, PFOA, PFBS, PFPeS, PFHxS, PFOS, FBSA and FHxSA were found in all samples. Individual PFAS concentration ranged from 3×10^{-3} to 260 μg/L and the mean concentration was the highest for FHxSA (44 ± 48 μg/L) and the lowest for MeFOSA (1×10^{-3} ± 4×10^{-3} μg/L). The pH value in all water samples ranged from 6.7 to 8.0. 21 of the PFAS exist in their deprotonated anionic forms (mean concentration of 140 ± 220 μg/L) while seven PFAS are non-ionic (mean concentration of 51 ± 54 μg/L). Please note that two zwitterionic PFAS (PBSaAm and PFHxSaAm) [43] were classified as non-ionic PFAS due to their overall neutral charge.

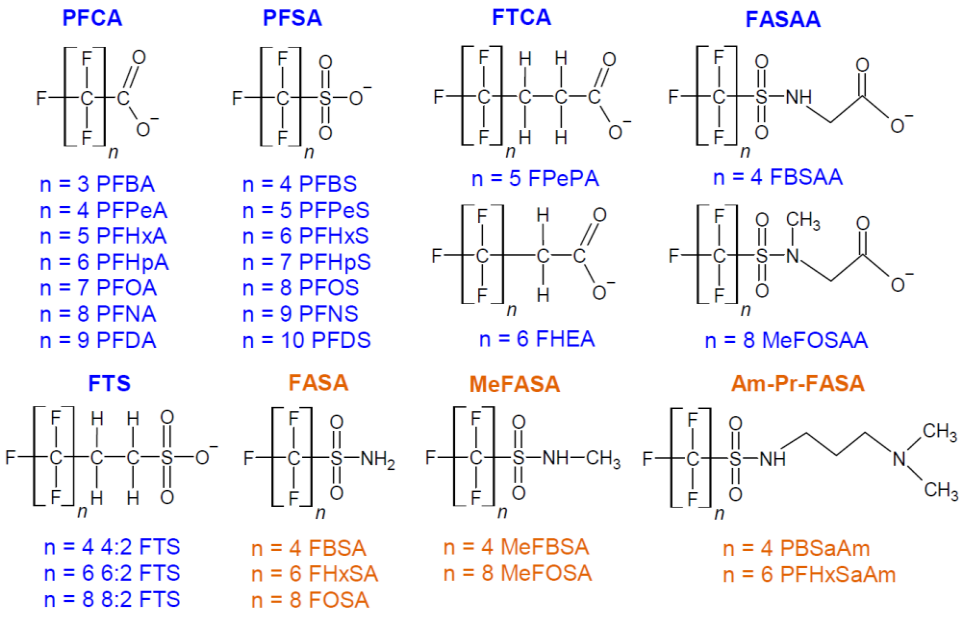

Figure 1. Structures of PFAS detected. Blue and orange fonts represent anionic and non-ionic PFAS, respectively, at the near neutral pH of all water samples. *n* represents individual C-F chain lengths. For reference, the detailed composition and concentration of individual PFAS is listed in **Tables S2** and **S5**, respectively.

The role of MOF structure. In our previous study we found that only MOFs with a combination of suitable (i) porosity and (ii) node composition (i.e., pore sizes exceeding the kinetic diameter of PFAS, and cationic metal nodes featuring terminally coordinating anionic ligands) exhibit significant adsorption capacities of anionic PFAA *via* an anion exchange mechanism.[25] However, the adsorption behavior of non-ionic PFAS on MOFs is unknown since for these interactions there is a lack of electrostatic attraction between adsorbents and adsorbates. To compare the role of MOF structure on anionic and non-ionic PFAS adsorption, MOFs NU-1000,[35] UiO-66,[36] and ZIF-8[37] with respective node compositions of $Zr_6(\mu_3\text{-}O)_4(\mu_3\text{-}OH)_4(H_2O)_4(OH)_4(\text{-}CO_2)_8$, $Zr_6(\mu_3\text{-}O)_4(\mu_3\text{-}OH)_4(\text{-}CO_2)_{12}$, and $Zn(\text{-}N)_4$ were used for the treatment of sample IDW 6. This sample was selected due to its high diversity and concentration of non-ionic PFAS as listed in **Tables S5**. A commercially available GAC was used for comparison in addition to a control that contained no adsorbent. **Figure 2** and **Table S6** display the structural features of respective MOFs and GAC used.

The detailed results of this adsorption study are represented in **Figures 3** and **S1-S4**. Each MOF was found to exhibit different adsorption selectivities towards the 21 PFAS tested in IDW 6. Per **Figure 3A**, NU-1000 shows high selectivity towards anionic PFAS (∑anionic PFAS removal capacity of 58%) and around quantitative selectivity towards non-ionic PFAS (∑non-ionic PFAS removal of 99%). UiO-66 exhibits similar removal characteristics for non-ionic PFAS (95% removal) but poor selectivity towards anionic PFAS (2% removal) while ZIF-8 features low affinity for both anionic and non-ionic PFAS (removal < 10%). GAC shows moderate selectivity for anionic and non-ionic PFAS with respective removal capacities of 37% and 44%. Noteworthy, the different selectivity towards anionic and non-ionic PFAS by different MOFs is independent of single PFAS concentrations and perfluorinated chain length/molecular size. All three MOF samples were characterized by powder X-ray diffraction (PXRD) to show that their structural integrity has not been compromised after adsorption testing. From respective PXRD patterns shown in **Figure S5** it is evident that NU-1000 and UiO-66 reveal an unchanged structural integrity while ZIF-8 shows some minor sings of degradation.[44]

The adsorption of anionic PFAS on NU-1000 was found in our earlier study to be dominated by ionic interactions.[25] We showed that the underlying adsorption mechanism can be described as an anion exchange reaction between the deprotonated carboxylic/sulfonic acid groups of PFAS and the terminally coordinated hydroxo ligands of NU-1000's Zr_6-node (for reference: $Zr_6(\mu_3\text{-}O)_4(\mu_3\text{-}OH)_4(H_2O)_4(OH)_4(\text{-}CO_2)_8$). Consequently, we postulate that a similar anion exchange mechanism leads to the high adsorption capacity of anionic PFCA, PFSA, FTCA, FTS, FASAA and Am-Pr-FASA (zwitterionic) in sample IDW 6. Hydrophobic interactions between the C-F chain of anionic PFAS molecules and the hydrophobic pockets formed by the pyrene-based ligands in NU-1000 also play a role in PFAS adsorption. Furthermore, according to Pearson's acid-base concept (i.e., HSAB theory), functional groups in anionic PFAS molecules such as sulfonates and carboxylates are considered hard bases and should interact strongly with hard acids such as the Zr_6-nodes. The high affinity for non-ionic FASA, Me-FASA, Am-Pr-FASA on NU-1000 can be explained by three potential mechanisms: (i) Pearson's HSAB theory which predicts that the amine groups of non-ionic PFAS (i.e., the hard base) should interact strongly with the Zr_6-nodes (i.e., the hard acid); (ii) Hydrophobic interaction between the C-F chain of non-ionic PFAS molecules and the hydrophobic pockets of NU-1000; and (iii) an alternative mechanism can be assumed from the amine groups of PFAS deprotonating the μ_3-bridging hydroxo groups of the Zr_6-nodes which can lead to strong electrostatic $\mu_3\text{-}O^{2-}\text{—}NH_3^+$ interactions. This chemistry has been described before by Sekizkardes *et. al*[45] for the reaction of alkylamines with polymers of intrinsic microporosity. Similar adsorption mechanisms can be assumed for the removal of PFAS using UiO-66. Its Zr_6-node does not possess any anion exchange capabilities (for reference: $Zr_6(\mu_3\text{-}O)_4(\mu_3\text{-}OH)_4(\text{-}CO_2)_{12}$, 12-connected node), therefore, resulting in only poor removal performance of anionic PFAS, while the overall general hardness and μ_3-briging hydroxo groups of the node promote high-capacity adsorption of non-ionic PFAS.

The amine groups of non-ionic PFAS can interact with at least the surface of fully saturated Zn-sites in ZIF-8. However, poor removal performance of both, anionic and non-ionic PFAS is observed for

ZIF-8 because its Zn-node also possess no anion exchange capability (for reference: $Zn(-N)_4$) and is also considered as a weak acid by Pearson.

The adsorption kinetics for the different adsorbents can be discussed from the PFAS removal efficiencies analyzed as a function of their adsorption time. As displayed in **Figures S1-S4** we found that the adsorption kinetics are different for each type of MOF which is likely related to their different pore apertures and pore sizes. Per **Figure S1**, they are the fastest for NU-1000 where the equilibrium of PFAS adsorption was reached within the first minute regardless of the charge state of PFAS as previously observed for anionic PFAS.[24] This performance significantly outperforms commercial GAC (equilibrium time > 48 h, **Figure S2**), ion exchange resins and other reported adsorbents.[25,46] However, it should be noted for reference that all sorbents studied exhibit different particle sizes as listed in **Table S6**. It is not considered in the discussion below, but these differences might also influence the sorbets' adsorption kinetics. The large diffusion-facilitating pores in NU-1000 feature one-dimensional hexagonal mesopores (33 Å) and one-dimensional triangular micropores (13 Å). Both pores are connected by 8 × 10 Å windows extending throughout the structure to facilitate rapid flow of substrates throughout the entire heterogeneous framework. For reference, the kinetic diameter of PFOS is in the range of 2.9 - 3.8 Å. In UiO-66, equilibrium of non-ionic PFAS adsorption is reached within the first 10 min (**Figure S3**) which is slower as compared to NU-1000. This observation is consistent with UiO-66's smaller pores featuring 7 Å apertures for its tetrahedral and octahedral cages of 8 and 11 Å in diameter, respectively. Similar findings were reported by Howarth *et al.* for the removal of selenite from water using NU-1000 and UiO-66.[47] ZIF-8 exhibits the slowest adsorption kinetics (> 30 min) of all MOFs tested (**Figure S4**) which can be attributed to the relatively small 3.4 Å pore aperture of its 13.4 Å-sized sodalite cages.[48]

In conclusion and as summarized in **Figure 3B**, higher adsorption capacities and kinetics for individual non-ionic PFAS are found for NU-1000 compared to UiO-66 and ZIF-8 due to their generally smaller pores and associated apertures. NU-1000 also features high affinities towards anionic PFAS due to its anion exchange capability which is non-existing for UiO-66 and ZIF-8. These combined features led us

to select NU-1000 as a probe to study the role of PFAS properties and water matrix on its adsorption behavior.

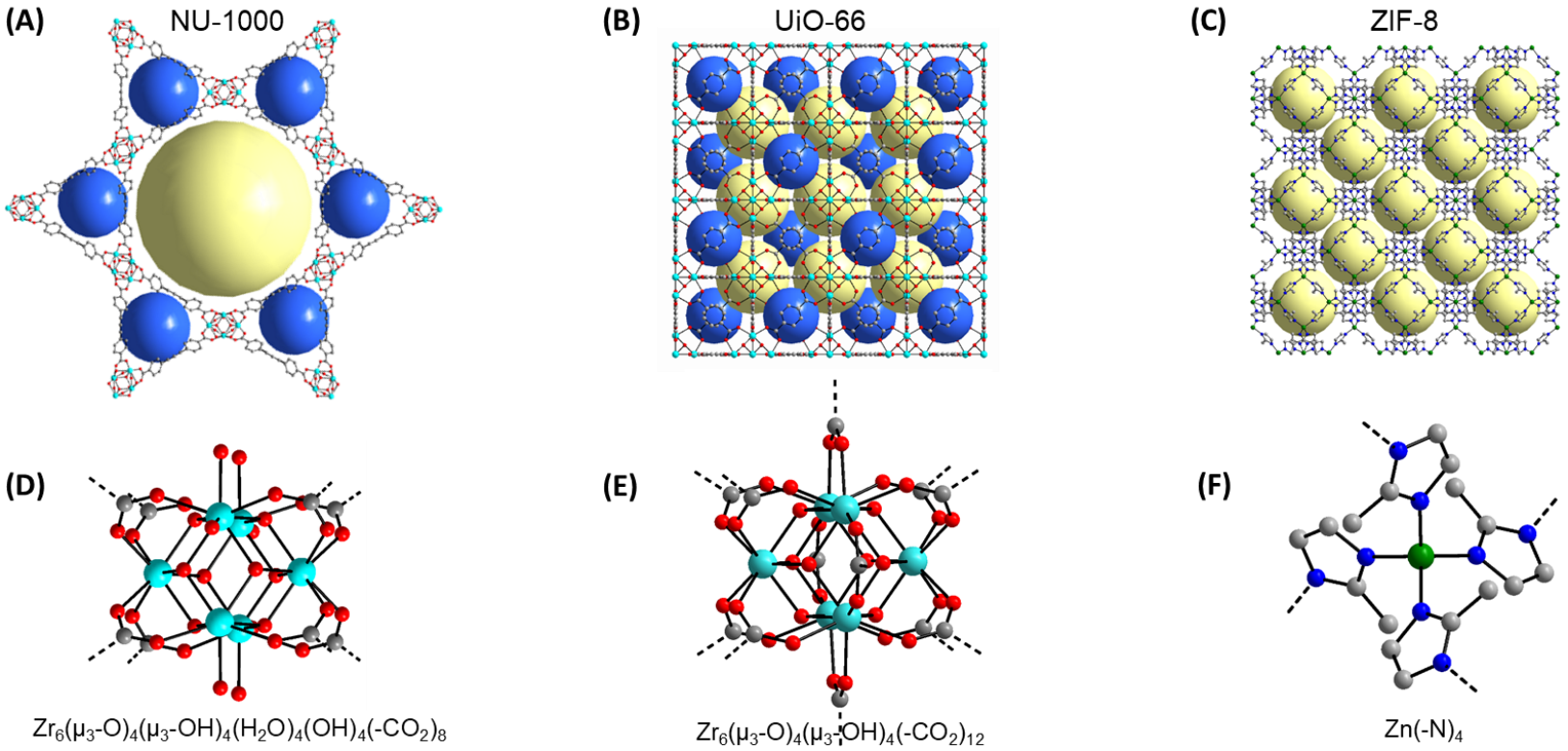

Figure 2. Crystal structures of MOFs NU-1000, UiO-66 and ZIF-8. (A-C) and (D-F) represent their packing diagrams and metal node compositions, respectively. Color scheme: carbon, gray; nitrogen, blue; oxygen, red; zirconium, turquoise; zinc, green. Hydrogen atoms are omitted for clarity and larger yellow and blue spheres represent the MOF's void spaces.

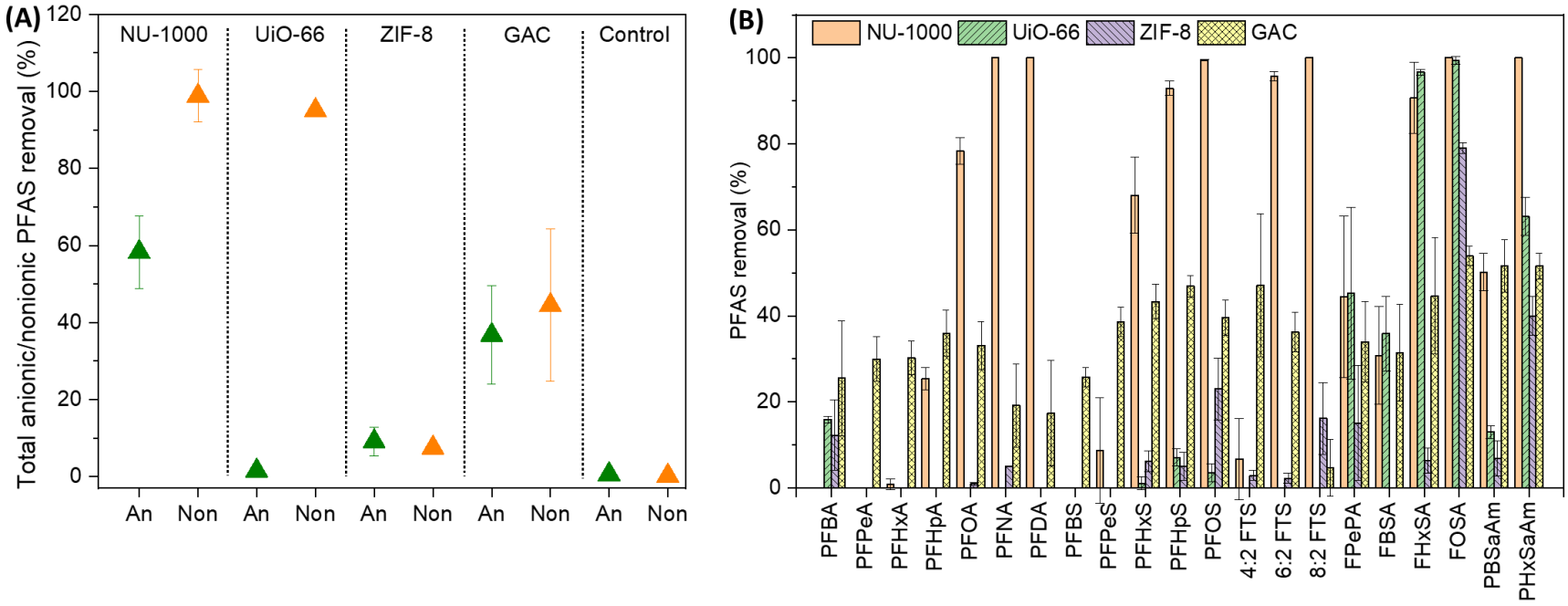

Figure 3. (A) Total anionic and non-ionic PFAS and (B) individual PFAS removal from IDW 6 using different adsorbents. The exposure time for NU-1000 was 30 min and that for UiO-66, ZIF-8, GAC and control (no adsorbent) was 48 h. Anionic PFAS include PFCAs, PFSAs, FTSs, FTCAs and FASAAs; non-ionic PFAS include FASAs, MeFASAs and Am-Pr-FASAs. Total anionic/non-ionic PFAS removal was calculated based on the difference of total anionic/non-ionic PFAS concentration before and after treatment. IDW 6 (pH of 6.9) was selected due to its higher number and concentration of non-ionic PFAS as shown in **Tables S5**. Some columns are not visible in (B) due to the small or zero values. For reference, the removal of individual PFAS from IDW 6 using different MOFs as a function of time can be found in **Figures S1-S4**.

The role of C-F chain length. Adsorption of 28 PFAS compounds from 11 IDW samples using NU-1000 was evaluated. All tested PFAS belong to a total of eight PFAS classes featuring each different C-F chain lengths (3-9 for PFCA; 4-10 for PFSA; 4, 6, and 8 for FTS; 5 and 6 for FTCA; 4 and 6 for FASAA; 4, 6 and 8 for FASA; 4 and 8 for MeFASA; 4 and 6 for Am-Pr-FASA). Systematic analysis of the adsorption results as displayed in **Figure 4** and listed in **Table S7** showing higher removal capacities for PFAS with longer C-F chain length from a total of six different PFAS classes, namely PFCA, PFSA, FTS, FASA, FASAA and Am-Pr-FASA. For example, in all 11 IDWs the mean removal of C5 (C-F chain length) PFHxA and C7 PFOA was 24 ± 35% and 80 ± 27%, respectively. However, it should be noted that per **Table S8**, the chain-length dependency for PFAS removal is independent of initial concentrations. For example, PFOA removal in IDWs 1 and 5 is constantly higher than PFHxA removal in those samples despite the higher concentration of PFHxA in IDW 2 and lower concentration in IDW 5. Another example of this chain length dependence is that C4 PBSaAm and C6 PHxSaAm of the Am-Pr-FASA class showed a mean removal of 43 ± 18% and 100 ± 0%, respectively. Such chain length dependency for PFAS removal from water was widely reported before for a multitude of adsorbents including GAC, IX resins, cyclodextrin polymers and nanotubes.[6,7] PFAS with longer perfluorocarbon chain exhibit higher hydrophobicity, thus, having lower water solubility and enhanced hydrophobic interactions between PFAS molecules and adsorbents (e.g., NU-1000 exhibits hydrophobic pockets due to its pyrene-based ligands). One exception of the chain length dependency is observed for FTCA where the removal of C5 FPePA and C6 FHEA was similar due to the longer C-H chain (one extra CH_2 unit) in C5 FPePA which leads to the similar hydrophobicity of C5 FPePA and C6 FHEA. Furthermore, C4 MeFBSA and C8 MeFOSA were only detected in IDWs 1 and 2, respectively, thus the removal of PFAS in the MeFASA class with different chain lengths cannot be compared.

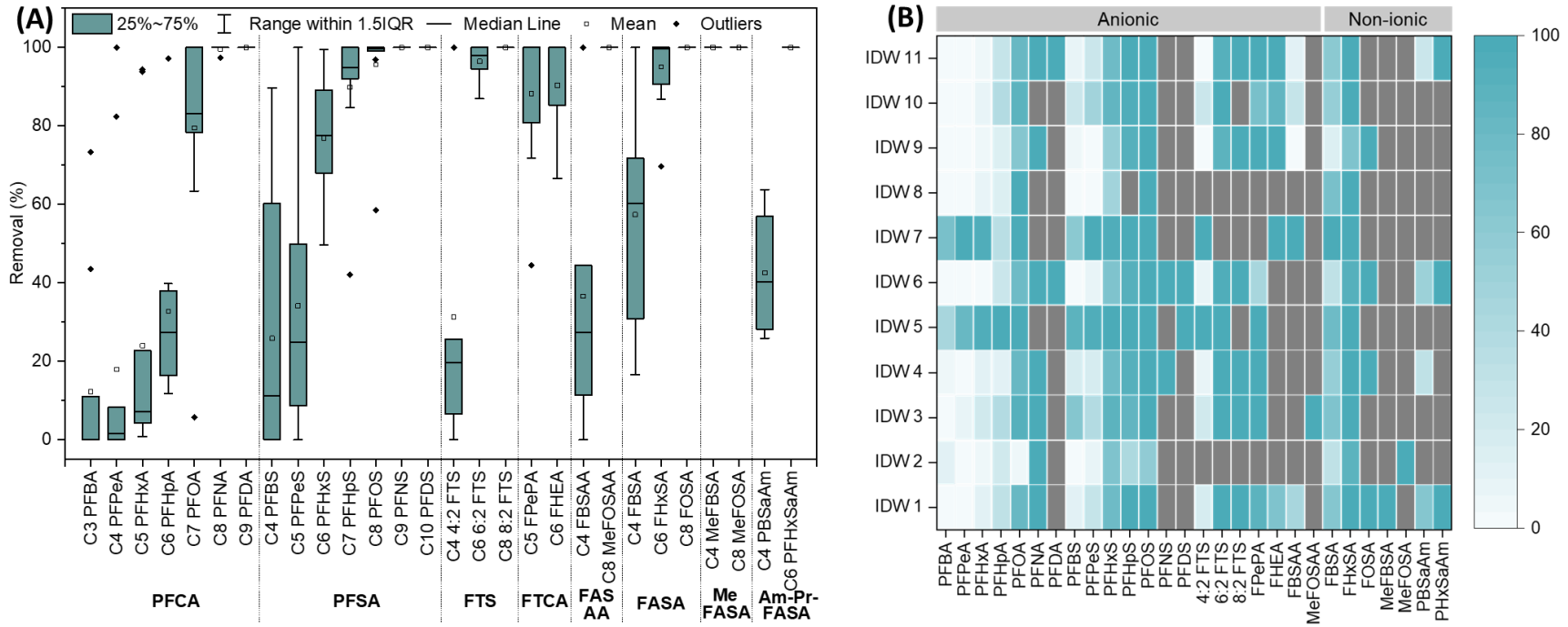

Figure 4. (A) Box chart and (B) heat map of individual PFAS removal from 11 IDW samples using NU-1000. Some boxes are not visible in (A) due to their small ranges of removal capacities. Color bar in (B) represents the removal in percentage and grey color indicates no PFAS detected. Anionic PFAS include PFCAs, PFSAs, FTSs, FTCAs and FASAAs; non-ionic PFAS include FASAs, MeFASAs and Am-Pr-FASAs. Experimental conditions: 50 mL IDWs, 10 mg NU-1000, and 30 min contact time. The removal of individual PFAS in IDWs is listed in **Table S7** for reference.

The role of functional group and charge state of PFAS. Eight PFAS classes were investigated to study the role of their functional group and charge state on their adsorption behavior. From **Figure 4** it is obvious that NU-1000 shows a consistently greater removal of PFSA than that of PFCA with the same perfluorocarbon chain length which is also widely observed for common adsorbents such as GAC, IX resin, zeolites, etc.[49] This observation is grounded in Person's HSAB principle which describes sulfonates as a harder base as compared to carboxylates.[50,51] NU-1000's Zr_6-node is considered a hard acid, and therefore, results in greater electrostatic interactions with sulfonates *vs.* carboxylates.[52] In addition, PFSA are generally more hydrophobic as compared to PFCA leading to more significant interactions with NU-1000's hydrophobic pockets.

While the PFAS community focuses primarily on the comparison of the adsorption properties of PFSA *vs.* PFCA, only little is known about the other > 5000 types of PFAS with a variety of functional groups which can alter their physiochemical properties (e.g., electronic and steric properties).[53] As displayed in **Figure 4B**, we found higher removal capacities for FTCA as compared to PFCA, and higher removal for FTS compared to PFSA (e.g., 78% and 93% in IDW 11 for C6 PFHxS and C6 6:2 FTS, respectively). This finding suggests that polyfluorinated compounds are removed to a larger extent than perfluorinated compounds with the same perfluorocarbon chain length which can be attributed to the higher hydrophobicity of polyfluorinated compounds with their extra CH_2 units.[54]

In addition, most PFAS studies generally probe the performance of adsorbents for anionic PFAS (e.g., PFOS and PFOA) removal but there are only limited reports on the adsorption of non-ionic PFAS.[7,55,56] We observed non-ionic FASA exhibiting higher removal compared to PFSA with the same perfluorocarbon chain length (e.g., C4, C6 and C8; 68% and 91% in IDW 6 for C6 PFHxS and C6 FHxSA, respectively). This preferential adsorption might be induced by FASA's amine group which is considered by Person a hard base resulting in strong interactions with NU-1000's Zr_6-node (a hard acid). [13,46,57]Thus, the higher removal for FASA compared to PFSA in this study indicates that the mechanism for non-ionic PFAS adsorption (with a sulfonamide functional group) is based on acid-base interactions while

hydrophobic interactions also play a role. Furthermore, **Figure 4B** shows that the PFAS removal capacities for FASA exceed that for FASAA (e.g., in IDWs 1, 10 and 11). This observation can be explained based on the different PFAS-NU-1000 interactions modes which are of a strong acid-base (i.e., Zr_6-amin) nature for FASA and of a relatively weak electrostatic (i.e., Zr_6-amide) nature for FASAA. In addition, amines are more basic as compared to amides and thus having the potential to deprotonate the μ_3-bridging hydroxo groups of the Zr_6-nodes resulting in strong O^{2-}—NH_3^+ electrostatic interactions. This acid-base reactivity is not possible for amides given their very low basicity. The opposite trend (FASAA > FASA) is reported for cyclodextrin polymers and activated carbons where FASAA's overall greater hydrophobicity and anionic carboxylate groups enhance the affinity for the adsorbents.[4] NU-1000's removal capacities for MeFASA and Am-Pr-FASA are higher compared to FASA with the same perfluorocarbon chain length due to their larger molecular sizes making them more hydrophobic. For example, C4 PBSaAm is consistently removed to a higher extent as compared to C4 FBSA in IDWs 6 and 11 where both PFAS are detected.

The role of water matrix. The conductivity (22-26000 μS/cm), TOC (0.11-268 mg/L), alkalinity (10-550 mg/L) and hardness (30-1130 mg/L) varied significantly for all tested IDWs. Their detailed characteristics are listed in **Tables S2** for reference. Given this complex composition of IDWs, these samples provided an ideal platform to investigate the role of water matrix on the MOF's PFAS removal performance. It is important to note that a statistical analysis revealed that the removal of PFAS was not significantly correlated with their initial concentrations ($p > 0.05$, **Table S8**). It is evident from **Figure 4B** that the removal of PFAS from IDWs varied significantly for anionic PFAS depending on the water matrix. The average removal capacities for anionic PFAS are the greatest for IDWs 5 and 7 with a mean removal of 93 ± 15% and 89 ± 21%. The lowest anionic PFAS removals are observed in IDWs 2 and 8-10 with a mean removal of 29 ± 34, 31 ± 42, 49 ± 45 and 53 ± 38 %, respectively.

The performance of adsorbents for PFAS removal from groundwater has been reported to be strongly associated with water chemistry (cations, anions, organic matters, etc.) *via* mechanisms including but not limited to (i) interrupting the interaction between adsorbents and adsorbates (e.g., competing for

adsorption sites on adsorbents); (ii) affecting the surface charge of adsorbates; and (iii) changing the hydrophobicity character.[34,49,55,58–60] The results of a statistical Spearman correlation analysis, listed in **Table S9**, reveal that the removal of anionic PFAS was significantly correlated (p-value < 0.05) with the total conductivity, alkalinity and hardness. TOC was negatively correlated (r-value < 0) with anionic PFAS removal; however, its role was not statistically significant (p > 0.05). For example, the conductivities are the lowest for IDWs 5 and 7 (25 and 22 μS/cm) and among the highest for IDWs 2 and 8-10 (>500 μS/cm) which is associated with higher PFAS removal in IDWs 5 and 7 and the lower removal in IDWs 2 and 8-10. As per **Figure 4B**, the removal efficiencies of individual anionic PFAS from IDW 5 are consistently higher (or equal when the removal reaches 100%) compared to that from IDW 10 (e.g., 97% and 94% in IDW 5, and 38% and 50% in IDW 10 for PFHpA and PFPeS, respectively). We showed in our previous study that the dominating mechanism for anionic PFAS (e.g., PFSA and PFCA) adsorption onto NU-1000 is based on an anion exchange mechanism featuring ionic interactions between the deprotonated acidic groups of PFAS and the formerly hydroxo-coordinated cationic Zr_6-nodes of NU-1000.[25] Thus, since groundwater with higher conductivity contains higher concentrations of inorganic ions (e.g., Cl^-, NO_3^-, CO_3^{2-}, etc.), these ions compete for the ion-exchange sites at the Zr_6-nodes leading to the lower anionic PFAS removal. Similarly, IDW 2, which exhibits the highest alkalinity (representative anions are HCO_3^-, CO_3^{2-}, OH^-) shows the lowest PFAS removal. These findings are consistent with those of other ion-exchange-based sorbents (e.g., boehmite, chitosan and resins) where the adsorption capacity of anionic PFAS has been revealed to be compromised by anionic co-contaminates.[7,26,34] Concurrently, the role of anions are reported to be insignificant on adsorbents which rely solely on hydrophobic interaction and/or hydrogen bonding.[49]

The concentration of cations also exhibits a strong negative correlation with PFAS adsorption for a variety of adsorbents (e.g., activated carbons, carbon nanotubes, alumina, and cyclodextrin polymers).[49,55,58] In this work, low PFAS removal in IDW 10 can be partially attributed to it having the highest total hardness among all IDWs (with most representative cations being Ca^{2+} and Mg^{2+}). Generally,

it is found that divalent cations (e.g., Ca^{2+} and Mg^{2+}) can bind with the anionic head groups of PFAS to form weak neutral complexes. These intermediates have the potential to weaken the electrostatic adsorbate-adsorbent interactions, thus, resulting in an overall decrease of PFAS adsorption.[55,59] However, for other adsorbents that respond to hydrophobic interactions as the dominant adsorption mechanism, the role of cations on PFAS adsorption is found to be insignificant.[49] Moreover, Jun *et al.* reported that divalent cations can act as bridges between neighboring anionic PFOA molecules thereby promoting the adsorption capacity of an Al-based MOF.[34] This finding, however, differs from what was observed in this work.

Organic (co-)contaminants are ubiquitous in groundwater and are considered another factor impacting PFAS adsorption.[49] For example, IDW 8 exhibits the highest TOC concentration (268 mg/L compared to 2.1 µg/L of total PFAS) resulting in a low mean PFAS removal capacity of 29 ± 34%. Multiple mechanisms can be responsible for this inhibition effect:[6] (i) ionic organic co-contaminants (e.g., humic acid) can compete with anionic PFAS for the ion exchange sites on MOFs;[56] (ii) hydrophobic organic co-contaminants can bind with MOFs *via* hydrophobic interaction and hydrogen bonding; (iii) strong basic functional groups on organic co-contaminants can facilitate acid-base interactions with the hard acid Zr_6-node; and (iv) macromolecular organic co-contaminants can compete for the adsorption of PFAS with the MOF *via* electrostatic and/or hydrophobic interaction.[7]

The adsorption of non-ionic PFAS was found to be negatively correlated with conductivity, total alkalinity, and total hardness ($r < 0$) and positively correlated with TOC ($r > 0$). However, these effects are not statistically significant ($p > 0.05$). **Figure 4B** shows that the removals for non-ionic PFAS are the highest for IDW 7 with a mean removal of 100 ± 0% and the lowest for IDW 9 with a mean removal of 62 ± 42%. For example, FHxSA, a non-ionic FASA detected in every groundwater sample, was 100% removed from IDW 8 which exhibited the highest TOC concentration and 100% removed from IDW 10 which exhibited the highest conductivity and total hardness. The water matrix lacking any influence on non-ionic PFAS removal further proved that non-ionic PFAS adsorption is dominated by acid-base interactions between PFAS's amine groups and NU-1000's Zr_6-nodes. In general, there is a very limited number of

investigations reported on the role of water matrix on non-ionic PFAS removal, especially in complex contaminated groundwater. For example, Ching *et al.* observed the adsorption of neutral PFAS using cyclodextrin polymers which was significantly inhibited in groundwater compared to nanopure water, which is different with the observations in this study for MOFs.[43]

Environmental implications. This study offers the first systematic investigation on the performance of emerging MOFs for the removal of different PFAS classes from a wide range of contaminated groundwater. The data revealed that the Zr-based MOF NU-1000 outperformed other MOFs with high affinity for both anionic and non-ionic PFAS. Our evidence shows that (i) electrostatic interactions between anionic PFAS and the cationic Zr_6 metal node of NU-1000 is the dominant mechanism for anionic PFAS adsorption and (ii) acid-base interactions between the amine groups of non-ionic PFAS and NU-1000's Zr_6-nodes are the key mechanism for non-ionic PFAS removal. Fundamental trends were observed showing preferred adsorption of long- over short-chain PFAS compounds, PFSA over PFCA, FASA over PFSA, FASA over FASAA, MeFASA over FASA, Am-Pr-FASA over FASA and polyfluorinated compounds over perfluorinated compounds with the same C-F chain length. The presence of inorganic cations, anions and organic co-contaminants demonstrated significant inhibitive effects on anionic PFAS adsorption on NU-1000 due to the competition for adsorption sites and/or weakening of the electrostatic status of PFAS among other mechanisms. The effect of water matrix was less pronounced for non-ionic PFAS. The present study supports the continued investigation of MOFs as promising platforms for the remediation of PFAS contaminated water; and significantly improves our understanding of PFAS adsorption performances and mechanisms of MOFs in a complex water matrix, paving the way for the design of more efficient MOFs for the adsorption of various PFAS classes.

SUPPORTING INFORMATION

Analytical method details; PXRD patterns of MOFs; IDW water sample characterizations; characterization details of adsorbents; removal efficiencies of PFAS from IDWs using different adsorbents; statistical analyses.

ACKNOWLEDGEMENTS

M.W. gratefully acknowledges the U.S. National Science Foundation CAREER Program (award no. 1752771) and the Clarkson/SUNY ESF Healthy Water Solutions Center of Excellence (CoE) for support of this research. T.M.H. gratefully thanks the support of Center for Air and Aquatic Resources Engineering and Sciences (CAARES), which is accredited to perform PFAS analysis by the U.S. Department of Defense Environmental Laboratory Accreditation Program (DoD ELAP). O.K.F. and T.I. gratefully acknowledge the support of the Nanoporous Materials Genome Center, funded by the U.S. Department of Energy (DOE), Office of Science, Basic Energy Sciences Program (award no. DE-FG02-17ER16362). R.L. gratefully thanks Junda Ren for the help in statistical analysis. In addition, we would like to thank GSI Environmental Inc. for groundwater sample collections and the U.S. Air Force for funding the sample collection (contract FA8903-17-C-0015).

REFERENCES

(1) Kaboré, H. A.; Vo Duy, S.; Munoz, G.; Méité, L.; Desrosiers, M.; Liu, J.; Sory, T. K.; Sauvé, S. Worldwide Drinking Water Occurrence and Levels of Newly-Identified Perfluoroalkyl and Polyfluoroalkyl Substances. *Sci. Total Environ.* **2018**, *616–617*, 1089–1100. https://doi.org/10.1016/j.scitotenv.2017.10.210.

(2) Kwiatkowski, C. F.; Andrews, D. Q.; Birnbaum, L. S.; Bruton, T. A.; DeWitt, J. C.; Knappe, D. R. U.; Maffini, M. V.; Miller, M. F.; Pelch, K. E.; Reade, A.; Soehl, A.; Trier, X.; Venier, M.;

Wagner, C. C.; Wang, Z.; Blum, A. Scientific Basis for Managing PFAS as a Chemical Class. *Environ. Sci. Technol. Lett.* **2020**, *7* (8), 532–543. https://doi.org/10.1021/acs.estlett.0c00255.

(3) Li, R.; Munoz, G.; Liu, Y.; Sauvé, S.; Ghoshal, S.; Liu, J. Transformation of Novel Polyfluoroalkyl Substances (PFASs) as Co-Contaminants during Biopile Remediation of Petroleum Hydrocarbons. *J. Hazard. Mater.* **2019**, *362*, 140–147. https://doi.org/https://doi.org/10.1016/j.jhazmat.2018.09.021.

(4) Wang, R.; Ching, C.; R. Dichtel, W.; E. Helbling, D. Evaluating the Removal of Per- and Polyfluoroalkyl Substances from Contaminated Groundwater with Different Adsorbents Using a Suspect Screening Approach. *Environ. Sci. Technol. Lett.* **2020**, *7* (12), 954–960. https://doi.org/10.1021/acs.estlett.0c00736.

(5) Singh, R. K.; Multari, N.; Nau-Hix, C.; Anderson, R. H.; Richardson, S. D.; Holsen, T. M.; Thagard, S. M. Rapid Removal of Poly- and Perfluorinated Compounds from Investigation-Derived Waste (IDW) in a Pilot-Scale Plasma Reactor. *Environ. Sci. Technol.* **2019**, *53* (19), 11375–11382. https://doi.org/10.1021/acs.est.9b02964.

(6) Gagliano, E.; Sgroi, M.; Falciglia, P. P.; Vagliasindi, F. G. A.; Roccaro, P. Removal of Poly- and Perfluoroalkyl Substances (PFAS) from Water by Adsorption: Role of PFAS Chain Length, Effect of Organic Matter and Challenges in Adsorbent Regeneration. *Water Res.* **2020**, *171*, 115381. https://doi.org/https://doi.org/10.1016/j.watres.2019.115381.

(7) Du, Z.; Deng, S.; Bei, Y.; Huang, Q.; Wang, B.; Huang, J.; Yu, G. Adsorption Behavior and Mechanism of Perfluorinated Compounds on Various Adsorbents—A Review. *J. Hazard. Mater.* **2014**, *274*, 443–454. https://doi.org/https://doi.org/10.1016/j.jhazmat.2014.04.038.

(8) Woodard, S.; Berry, J.; Newman, B. Ion Exchange Resin for PFAS Removal and Pilot Test Comparison to GAC. *Remediat. J.* **2017**, *27* (3), 19–27. https://doi.org/https://doi.org/10.1002/rem.21515.

(9) Park, M.; Wu, S.; Lopez, I. J.; Chang, J. Y.; Karanfil, T.; Snyder, S. A. Adsorption of Perfluoroalkyl Substances (PFAS) in Groundwater by Granular Activated Carbons: Roles of

Hydrophobicity of PFAS and Carbon Characteristics. *Water Res.* **2020**, *170*, 115364. https://doi.org/https://doi.org/10.1016/j.watres.2019.115364.

(10) Kennedy, A. M.; Reinert, A. M.; Knappe, D. R. U.; Ferrer, I.; Summers, R. S. Full- and Pilot-Scale GAC Adsorption of Organic Micropollutants. *Water Res.* **2015**, *68*, 238–248. https://doi.org/https://doi.org/10.1016/j.watres.2014.10.010.

(11) Haddad, M.; Oie, C.; Vo Duy, S.; Sauvé, S.; Barbeau, B. Adsorption of Micropollutants Present in Surface Waters onto Polymeric Resins: Impact of Resin Type and Water Matrix on Performance. *Sci. Total Environ.* **2019**, *660*, 1449–1458. https://doi.org/https://doi.org/10.1016/j.scitotenv.2018.12.247.

(12) Zhang, D. Q.; Zhang, W. L.; Liang, Y. N. Adsorption of Perfluoroalkyl and Polyfluoroalkyl Substances (PFASs) from Aqueous Solution - A Review. *Sci. Total Environ.* **2019**, *694*, 133606. https://doi.org/https://doi.org/10.1016/j.scitotenv.2019.133606.

(13) Drout, R. J.; Robison, L.; Chen, Z.; Islamoglu, T.; Farha, O. K. Zirconium Metal–Organic Frameworks for Organic Pollutant Adsorption. *Trends Chem.* **2019**, *1* (3), 304–317. https://doi.org/https://doi.org/10.1016/j.trechm.2019.03.010.

(14) An, W.; Aulakh, D.; Zhang, X.; Verdegaal, W.; R. Dunbar, K.; Wriedt, M. Switching of Adsorption Properties in a Zwitterionic Metal–Organic Framework Triggered by Photogenerated Radical Triplets. *Chem. Mater.* **2016**, *28* (21), 7825–7832. https://doi.org/10.1021/acs.chemmater.6b03224.

(15) Aulakh, D.; R. Varghese, J.; Wriedt, M. A New Design Strategy to Access Zwitterionic Metal–Organic Frameworks from Anionic Viologen Derivates. *Inorg. Chem.* **2015**, *54* (4), 1756–1764. https://doi.org/10.1021/ic5026813.

(16) Aulakh, D.; Xie, H.; Shen, Z.; Harley, A.; Zhang, X.; A. Yakovenko, A.; R. Dunbar, K.; Wriedt, M. Systematic Investigation of Controlled Nanostructuring of Mn12 Single-Molecule Magnets Templated by Metal–Organic Frameworks. *Inorg. Chem.* **2017**, *56* (12), 6965–6972. https://doi.org/10.1021/acs.inorgchem.7b00514.

(17) Aulakh, D.; B. Pyser, J.; Zhang, X.; A. Yakovenko, A.; R. Dunbar, K.; Wriedt, M. Metal–Organic Frameworks as Platforms for the Controlled Nanostructuring of Single-Molecule Magnets. *J. Am. Chem. Soc.* **2015**, *137* (29), 9254–9257. https://doi.org/10.1021/jacs.5b06002.

(18) Aulakh, D.; R. Varghese, J.; Wriedt, M. The Importance of Polymorphism in Metal–Organic Framework Studies. *Inorg. Chem.* **2015**, *54* (17), 8679–8684. https://doi.org/10.1021/acs.inorgchem.5b01311.

(19) Ji, Z.; Li, T.; Yaghi, O. M. Sequencing of Metals in Multivariate Metal-Organic Frameworks. *Science.* **2020**, *369* (6504), 674–680. https://doi.org/10.1126/science.aaz4304.

(20) Wen, Y.; Zhang, P.; Sharma, V. K.; Ma, X.; Zhou, H.-C. Metal-Organic Frameworks for Environmental Applications. *Cell Reports Phys. Sci.* **2021**, *2* (2), 100348. https://doi.org/https://doi.org/10.1016/j.xcrp.2021.100348.

(21) Wang, T.; Peng, Y.-L.; Lin, E.; Niu, Z.; Li, P.; Ma, S.; Zhao, P.; Chen, Y.; Cheng, P.; Zhang, Z. Robust Bimetallic Ultramicroporous Metal–Organic Framework for Separation and Purification of Noble Gases. *Inorg. Chem.* **2020**, *59* (7), 4868–4873. https://doi.org/10.1021/acs.inorgchem.0c00134.

(22) Dong, Q.; Zhang, X.; Liu, S.; Lin, R.-B.; Guo, Y.; Ma, Y.; Yonezu, A.; Krishna, R.; Liu, G.; Duan, J.; Matsuda, R.; Jin, W.; Chen, B. Tuning Gate-Opening of a Flexible Metal–Organic Framework for Ternary Gas Sieving Separation. *Angew. Chemie Int. Ed.* **2020**, *59* (50), 22756–22762. https://doi.org/https://doi.org/10.1002/anie.202011802.

(23) Hasan, Z.; Jhung, S. H. Removal of Hazardous Organics from Water Using Metal-Organic Frameworks (MOFs): Plausible Mechanisms for Selective Adsorptions. *J. Hazard. Mater.* **2015**, *283*, 329–339. https://doi.org/https://doi.org/10.1016/j.jhazmat.2014.09.046.

(24) Kobielska, P. A.; Howarth, A. J.; Farha, O. K.; Nayak, S. Metal–Organic Frameworks for Heavy Metal Removal from Water. *Coord. Chem. Rev.* **2018**, *358*, 92–107. https://doi.org/https://doi.org/10.1016/j.ccr.2017.12.010.

(25) Li, R.; Alomari, S.; Stanton, R.; Wasson, M. C.; Islamoglu, T.; Farha, O. K.; Holsen, T. M.;

Thagard, S. M.; Trivedi, D. J.; Wriedt, M. Efficient Removal of Per- And Polyfluoroalkyl Substances from Water with Zirconium-Based Metal-Organic Frameworks. *Chem. Mater.* **2021**, *33* (9), 3276–3285. https://doi.org/10.1021/acs.chemmater.1c00324.

(26) Clark, C.; A.; N. Heck, K.; D. Powell, C.; S. Wong, M. Highly Defective UiO-66 Materials for the Adsorptive Removal of Perfluorooctanesulfonate. *ACS Sustain. Chem. Eng.* **2019**, *7* (7), 6619–6628. https://doi.org/10.1021/acssuschemeng.8b05572.

(27) Liu, K.; Zhang, S.; Hu, X.; Zhang, K.; Roy, A.; Yu, G. Understanding the Adsorption of PFOA on MIL-101(Cr)-Based Anionic-Exchange Metal–Organic Frameworks: Comparing DFT Calculations with Aqueous Sorption Experiments. *Environ. Sci. Technol.* **2015**, *49* (14), 8657–8665. https://doi.org/10.1021/acs.est.5b00802.

(28) Barpaga, D.; Zheng, J.; Sung Han, K.; A. Soltis, J.; Shutthanandan, V.; Basuray, S.; Peter McGrail, B.; Chatterjee, S.; Kishan Motkuri, R. Probing the Sorption of Perfluorooctanesulfonate Using Mesoporous Metal–Organic Frameworks from Aqueous Solutions. *Inorg. Chem.* **2019**, *58* (13), 8339–8346. https://doi.org/10.1021/acs.inorgchem.9b00380.

(29) Sini, K.; Bourgeois, D.; Idouhar, M.; Carboni, M.; Meyer, D. Metal–Organic Framework Sorbents for the Removal of Perfluorinated Compounds in an Aqueous Environment. *New J. Chem.* **2018**, *42* (22), 17889–17894. https://doi.org/10.1039/C8NJ03312A.

(30) Chen, M. J.; Yang, A. C.; Wang, N. H.; Chiu, H. C.; Li, Y. L.; Kang, D. Y.; Lo, S. L. Influence of Crystal Topology and Interior Surface Functionality of Metal-Organic Frameworks on PFOA Sorption Performance. *Microporous Mesoporous Mater.* **2016**, *236*, 202–210. https://doi.org/https://doi.org/10.1016/j.micromeso.2016.08.046.

(31) Li, Y.; Yang, Z.; Wang, Y.; Bai, Z.; Zheng, T.; Dai, X.; Liu, S.; Gui, D.; Liu, W.; Chen, M.; Chen, L.; Diwu, J.; Zhu, L.; Zhou, R.; Chai, Z.; Albrecht-Schmitt, T. E.; Wang, S. A Mesoporous Cationic Thorium-Organic Framework That Rapidly Traps Anionic Persistent Organic Pollutants. *Nat. Commun.* **2017**, *8* (1), 1354. https://doi.org/10.1038/s41467-017-01208-w.

(32) Yang, Y.; Zheng, Z.; Ji, W.; Xu, J.; Zhang, X. Insights to Perfluorooctanoic Acid Adsorption

Micro-Mechanism over Fe-Based Metal Organic Frameworks: Combining Computational Calculation with Response Surface Methodology. *J. Hazard. Mater.* **2020**, *395*, 122686. https://doi.org/https://doi.org/10.1016/j.jhazmat.2020.122686.

(33) Zhao, C.; Xu, Y.; Xiao, F.; Ma, J.; Zou, Y.; Tang, W. Perfluorooctane Sulfonate Removal by Metal-Organic Frameworks (MOFs): Insights into the Effect and Mechanism of Metal Nodes and Organic Ligands. *Chem. Eng. J.* **2021**, *406*, 126852. https://doi.org/https://doi.org/10.1016/j.cej.2020.126852.

(34) Jun, B. M.; Hwang, H. S.; Heo, J.; Han, J.; Jang, M.; Sohn, J.; Park, C. M.; Yoon, Y. Removal of Selected Endocrine-Disrupting Compounds Using Al-Based Metal Organic Framework: Performance and Mechanism of Competitive Adsorption. *J. Ind. Eng. Chem.* **2019**, *79*, 345–352. https://doi.org/https://doi.org/10.1016/j.jiec.2019.07.009.

(35) E. Mondloch, J.; Bury, W.; Fairen-Jimenez, D.; Kwon, S.; J. DeMarco, E.; H. Weston, M.; A. Sarjeant, A.; T. Nguyen, S.; C. Stair, P.; Q. Snurr, R.; K. Farha, O.; T. Hupp, J. Vapor-Phase Metalation by Atomic Layer Deposition in a Metal–Organic Framework. *J. Am. Chem. Soc.* **2013**, *135* (28), 10294–10297. https://doi.org/10.1021/ja4050828.

(36) Cavka, J. H.; Jakobsen, S.; Olsbye, U.; Guillou, N.; Lamberti, C.; Bordiga, S.; Lillerud, K. P. A New Zirconium Inorganic Building Brick Forming Metal Organic Frameworks with Exceptional Stability. *J. Am. Chem. Soc.* **2008**, *130* (42), 13850–13851. https://doi.org/10.1021/ja8057953.

(37) Park, K. S.; Ni, Z.; Cô, A. P.; Choi, J. Y.; Huang, R.; Uribe-Romo, F. J.; Chae, H. K.; O'keeffe, M.; Yaghi, O. M. Exceptional Chemical and Thermal Stability of Zeolitic Imidazolate Frameworks. *Proc. Natl. Acad. Sci.* **2006**, *103* (27), 10186–10191.

(38) Katz, M. J.; Brown, Z. J.; Colón, Y. J.; Siu, P. W.; Scheidt, K. A.; Snurr, R. Q.; Hupp, J. T.; Farha, O. K. A Facile Synthesis of UiO-66, UiO-67 and Their Derivatives. *Chem. Commun.* **2013**, *49* (82), 9449–9451. https://doi.org/10.1039/C3CC46105J.

(39) Planas, N.; E. Mondloch, J.; Tussupbayev, S.; Borycz, J.; Gagliardi, L.; T. Hupp, J.; K. Farha, O.; J. Cramer, C. Defining the Proton Topology of the Zr6-Based Metal–Organic Framework NU-

1000. *J. Phys. Chem. Lett.* **2014**, *5* (21), 3716–3723. https://doi.org/10.1021/jz501899j.

(40) Jian, M.; Liu, B.; Liu, R.; Qu, J.; Wang, H.; Zhang, X. Water-Based Synthesis of Zeolitic Imidazolate Framework-8 with High Morphology Level at Room Temperature. *RSC Adv.* **2015**, *5*, 48433–48441. https://doi.org/10.1039/c5ra04033g.

(41) Britt, D.; Furukawa, H.; Wang, B.; Glover, T. G.; Yaghi, O. M. Highly Efficient Separation of Carbon Dioxide by a Metal-Organic Framework Replete with Open Metal Sites. *Proc. Natl. Acad. Sci.* **2009**, *106* (49), 20637–20640.

(42) Islamoglu, T.; Otake, K.; Li, P.; Buru, C. T.; Peters, A. W.; Akpinar, I.; Garibay, S. J.; Farha, O. K. Revisiting the Structural Homogeneity of NU-1000, a Zr-Based Metal–Organic Framework. *Cryst Eng Comm* **2018**, *20* (39), 5913–5918. https://doi.org/10.1039/C8CE00455B.

(43) Ching, C.; J. Klemes, M.; Trang, B.; R. Dichtel, W.; E. Helbling, D. β-Cyclodextrin Polymers with Different Cross-Linkers and Ion-Exchange Resins Exhibit Variable Adsorption of Anionic, Zwitterionic, and Nonionic PFASs. *Environ. Sci. Technol.* **2020**, *54* (19), 12693–12702. https://doi.org/10.1021/acs.est.0c04028.

(44) Zhang, H.; Liu, D.; Yao, Y.; Zhang, B.; Lin, Y. S. Stability of ZIF-8 Membranes and Crystalline Powders in Water at Room Temperature. *J. Memb. Sci.* **2015**, *485*, 103–111. https://doi.org/https://doi.org/10.1016/j.memsci.2015.03.023.

(45) Sekizkardes, A. K.; Hammache, S.; Hoffman, J. S.; Hopkinson, D. Polymers of Intrinsic Microporosity Chemical Sorbents Utilizing Primary Amine Appendance Through Acid–Base and Hydrogen-Bonding Interactions. *ACS Appl. Mater. Interfaces* **2019**, *11* (34), 30987–30991. https://doi.org/10.1021/acsami.9b09856.

(46) Hamisu, A. M.; Ariffin, A.; Wibowo, A. C. Cation Exchange in Metal-Organic Frameworks (MOFs): The Hard-Soft Acid-Base (HSAB) Principle Appraisal. *Inorganica Chim. Acta* **2020**, *511*, 119801. https://doi.org/https://doi.org/10.1016/j.ica.2020.119801.

(47) Howarth, A. J.; Katz, M. J.; Wang, T. C.; Platero-Prats, A. E.; Chapman, K. W.; Hupp, J. T.; Farha, O. K. High Efficiency Adsorption and Removal of Selenate and Selenite from Water Using

Metal-Organic Frameworks. *J. Am. Chem. Soc.* **2015**, *137* (23), 7488–7494. https://doi.org/10.1021/jacs.5b03904.

(48) Gao, P.; Shi, X.; Xu, X.; Wei, W. Versatile and Efficient Mechanochemical Synthesis of Crystalline Guest⊂Zeolitic Imidazolate Framework Complexes by in Situ Host–Guest Nanoconfinement. *Cryst. Growth Des.* **2018**, *18* (10), 5845–5852. https://doi.org/10.1021/acs.cgd.8b00528.

(49) Wu, C.; Klemes, M. J.; Trang, B.; Dichtel, W. R.; Helbling, D. E. Exploring the Factors That Influence the Adsorption of Anionic PFAS on Conventional and Emerging Adsorbents in Aquatic Matrices. *Water Res.* **2020**, *182*, 115950. https://doi.org/10.1016/j.watres.2020.115950.

(50) H. Walters, F. Design of Corrosion Inhibitors: Use of the Hard and Soft Acid-Base (HSAB) Theory. *J. Chem. Educ.* **1991**, *68* (1). https://doi.org/10.1021/ed068p29.

(51) Snoeyink, V.; Jenkins, D. JenkinsD. Water Chemistry. New York: John Wiley & Sons 1980.

(52) McCleaf, P.; Englund, S.; Östlund, A.; Lindegren, K.; Wiberg, K.; Ahrens, L. Removal Efficiency of Multiple Poly- and Perfluoroalkyl Substances (PFASs) in Drinking Water Using Granular Activated Carbon (GAC) and Anion Exchange (AE) Column Tests. *Water Res.* **2017**, *120*, 77–87. https://doi.org/https://doi.org/10.1016/j.watres.2017.04.057.

(53) Park, M.; Daniels, K. D.; Wu, S.; Ziska, A. D.; Snyder, S. A. Magnetic Ion-Exchange (MIEX) Resin for Perfluorinated Alkylsubstance (PFAS) Removal in Groundwater: Roles of Atomic Charges for Adsorption. *Water Res.* **2020**, *181*, 115897. https://doi.org/10.1016/j.watres.2020.115897.

(54) Ateia, M.; F. Attia, M.; Maroli, A.; Tharayil, N.; Alexis, F.; C. Whitehead, D.; Karanfil, T. Rapid Removal of Poly- and Perfluorinated Alkyl Substances by Poly(Ethylenimine)-Functionalized Cellulose Microcrystals at Environmentally Relevant Conditions. *Environ. Sci. & Technol. Lett.* **2018**, *5* (12), 764–769. https://doi.org/10.1021/acs.estlett.8b00556.

(55) Wang, F.; Shih, K. Adsorption of Perfluorooctanesulfonate (PFOS) and Perfluorooctanoate (PFOA) on Alumina: Influence of Solution PH and Cations. *Water Res.* **2011**, *45* (9), 2925–2930.

https://doi.org/10.1016/j.watres.2011.03.007.

(56) Maimaiti, A.; Deng, S.; Meng, P.; Wang, W.; Wang, B.; Huang, J.; Wang, Y.; Yu, G. Competitive Adsorption of Perfluoroalkyl Substances on Anion Exchange Resins in Simulated AFFF-Impacted Groundwater. *Chem. Eng. J.* **2018**, *348*, 494–502. https://doi.org/10.1016/j.cej.2018.05.006.

(57) Pankajakshan, A.; Sinha, M.; Ojha, A. A.; Mandal, S. Water-Stable Nanoscale Zirconium-Based Metal−Organic Frameworks for the Effective Removal of Glyphosate from Aqueous Media. *ACS Omega* **2018**, *3*, 7832–7839. https://doi.org/10.1021/acsomega.8b00921.

(58) Kwadijk, C. J. A. F.; Velzeboer, I.; Koelmans, A. A. Sorption of Perfluorooctane Sulfonate to Carbon Nanotubes in Aquatic Sediments. *Chemosphere* **2013**, *90* (5), 1631–1636. https://doi.org/10.1016/j.chemosphere.2012.08.041.

(59) Jeon, J.; Kannan, K.; Lim, B. J.; An, K. G.; Kim, S. D. Effects of Salinity and Organic Matter on the Partitioning of Perfluoroalkyl Acid (PFAs) to Clay Particles. *J. Environ. Monit.* **2011**, *13* (6), 1803–1810. https://doi.org/10.1039/C0EM00791A.

(60) Yan, B.; Munoz, G.; Sauvé, S.; Liu, J. Molecular Mechanisms of Per- and Polyfluoroalkyl Substances on a Modified Clay: A Combined Experimental and Molecular Simulation Study. *Water Res.* **2020**, *184*, 116166. https://doi.org/https://doi.org/10.1016/j.watres.2020.116166.

TOC graphic

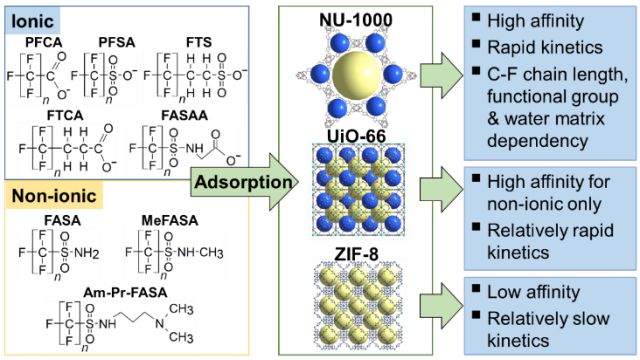
Ionic
PFCA
PFSA
FTS
FTCA
FASAA
Non-ionic
FASA
MeFASA
Am-Pr-FASA
Adsorption
NU-1000
UiO-66
ZIF-8
High affinity
Rapid kinetics
C-F chain length, functional group & water matrix dependency
High affinity for non-ionic only
Relatively rapid kinetics
Low affinity
Relatively slow kinetics